

COMMON-VIEW GPS TIME TRANSFER ACCURACY AND STABILITY RESULTS

James R. Semler
Interstate Electronics Corporation
1001 E. Ball Road
Anaheim, California 92803

Abstract

This paper presents the results of time and frequency dissemination research at Interstate Electronics that achieves 10-nanosecond timing accuracy and stability of parts in 10^{14} over continental baselines. Global Positioning System (GPS) receiver data is processed by a differential, common-view technique that cancels most of the cardinal errors. We characterize the noise in the GPS data by using multicorner-hat separation-of-variances techniques. These noise values set Kalman smoother parameters for removal of random noise in the common-view data. The disagreement between various satellite measurements provides a measure of common-view GPS accuracy.

We present a summary of the analytical concepts, followed by the results of real-world data processing in common-view tests between Interstate/Anaheim and the United States Naval Observatory (USNO). The results of side-by-side GPS receiver testing, using the algorithms described here, provide measurements of GPS receiver stability, which can reach levels of 1 nanosecond per sidereal day.

INTRODUCTION — WHAT AND WHY

Although navigation, testing, and sensor data gathering have often required precise, stable time maintenance, currently implemented technology lacks the accuracy required by new military program demands. Correlation of signals recorded by remote sensor data gathering systems needs highly accurate synchronization of several remote sites' frequency standards. Some systems demand synchronization accuracies of 10-nanosecond error or better for meeting their requirements. Testing applications also impose stringent synchronization and time stability requirements, particularly with the Global Positioning System (GPS).

Validation of state-of-the-art time and frequency dissemination accuracy and stability demands "prior-free" analysis techniques that do not depend on a predetermined system model nor the availability of a superior reference clock. The introduction of such a reference merely begs the question, as the reference itself may be invalid. "Who checks the checker?" Other programs demanding high instrumentation accuracy have faced similar problems in validation. The current performance analysis methodology used for GPS, Trident II, and similar navigation/time systems, however, lacks the capability to provide independent estimates of time stability without prior modeling. Kalman filtering and maximum-likelihood estimation require elaborate models for accurate performance estimation. However, they fail to provide parameters needed in the model description, such as GPS clock noise variances. Current accuracy validation techniques implement systems or clocks that must be several times more accurate than the system under test. The technique cannot by itself validate the accuracy of the so-called reference, thus casting doubt on the analysis results.

The long-term stability of GPS-based time and frequency dissemination depends on the long-term repeatability of the GPS ranging signal delays. As such, a GPS receiver designed for precise time transfer has different design priorities from one designed for dynamic navigation. Hence, military users of GPS have not yet reaped all the benefits of the extensive time and frequency dissemination research by the civil and academic communities. Existing military GPS receiver designs emphasize ruggedness, antijam capability, and Kalman-based navigation data processing. These considerations conflict with long-term receiver delay stability needed for precise time maintenance.

To provide cost-effective solutions to these problems, Interstate Electronics Corporation (IEC) has developed the needed time and frequency dissemination technology and performance analysis techniques in support of numerous military applications. In 1989 we completed the program initiated in August 1988 to:

- Demonstrate remote clock synchronization accurate to within 10 nanoseconds or less in real-world testing over baselines ranging from zero to continental distances.
- Develop, implement, and test prior-free algorithms that estimate the stability of each component of a time and frequency dissemination system based on GPS measurements.

To achieve these objectives, we have been:

- Conducting GPS common-view time transfer tests to validate the 10-nanosecond accuracy over a continental baseline.
- Performing GPS common-view time transfer tests over a zero baseline to measure receiver delay stability.
- Implementing the latest multicorner hat separation algorithms to provide quantitative GPS system clock noise variance estimates.
- Teaming with the Time and Frequency Division experts at the National Institute of Standards and Technology (NIST) in developing and implementing these approaches.

COMMON-VIEW GPS — APPROACH AND RESULTS

Our time transfer approach uses a single GPS satellite in common view from two clock locations to provide error cancellations, even over large baselines, which permit us to achieve the accuracy goal. Radio techniques using WWV or WWVH, LORAN, portable clock trips, or single-view GPS do not meet our goals. Timing using the Space Shuttle or laser-based systems is prohibitively expensive^[1]. Thus GPS common view emerged as the most cost-effective solution.

Two stations equipped with GPS receivers can compare their local time standards to nanosecond-level errors by tracking the same satellite simultaneously, and then differencing the measured local time offsets with respect to GPS time. This differential processing cancels most of the major GPS error sources. Variations on this technique allow us to compute the long-term stability of GPS receivers in the Interstate GPS laboratory.

The GPS consists of three segments: space, control, and user. The space segment contains several satellites in semisynchronous orbits that have ground tracks repeating each sidereal day. These satellites emit an RF signal consisting of a carrier wave modulated by a pseudorandom code and a navigation message. The control segment tracks these signals, determines the satellite orbit and clock offset parameters, and uploads these data to each satellite. However, the control segment orbit determination introduces satellite position and time errors into the uploaded data. The user segment

also tracks the satellites, demodulates the orbital data, and computes position and time from the range measurements. These measurements are taken by time-correlation of the pseudorandom code received from the satellite with a copy generated by the user equipment. Because the correlation process introduces the user clock error into the transit time measurement, the user must also solve for time errors. The four variables, three position coordinates and one time correction, require four correlation measurements for a fully determined solution. If the user equipment stores its presurveyed position, then GPS time can be obtained by tracking only one satellite.

Users needing to synchronize their clocks can do so by taking measurements against the GPS time scale and then differencing their local clock offsets from that time scale. If two users agree to track a satellite in common view from both sites simultaneously, the differencing cancels most of the GPS measurement errors, as shown in Figure 1.

The GPS measurements contain several errors from satellite orbit and clock corrections, ionospheric and tropospheric effects, user-surveyed position, and receiver delays. Some errors can, however, be removed. Satellite clock correction error drops out completely because its effect on ranging error is identical in both time offset measurements. The satellite orbital errors project into range measurements as shown in Table 1. When common view satellite measurements are differenced, however, the orbital error cancels to the magnitude of the difference of the projections. The extent of this cancellation depends on the distance between the receivers. The orbital error can dominate the other errors in a common-view GPS measurement if the distance between the receivers is very large, such as intercontinental distances.

Although the common-view technique removes the largest portion of GPS time offset measurement error, some error sources are not reduced by this practice. Ionospheric delays pose particular problems. Unless dual-frequency measurements are available, the user must rely on the broadcast single-frequency model. This model removes only 50 percent of the overall ionospheric error. Common-view measurements over baselines less than 1,000 kilometers, however, tend to remove most of the residual ionospheric errors. Further suppression of the ionospheric error occurs if measurements are taken at night during low ionospheric activity. Tropospheric models provide accuracies less than 1 foot in range, as demonstrated in Reference 2. Errors in receiver coordinate surveys introduce ranging errors similar to ephemeris errors.

The repeatability of the common-view GPS measurement accuracy pivots on the repeatability of receiver delays. Because of the differential comparisons, the magnitude of the delay does not matter so long as the delay is calibrated relative to the other GPS receivers used in common view and that delay remains the same from day to day. Short-term noise introduced by the tracking loops is suppressed by least-squares fitting of raw ranging data. The long-term delay variation depends on RF filter bandwidth, architecture, and environmental sensitivity. Typically the delay variation is a percentage of the absolute delay. For example, a receiver with 100 nanoseconds of delay experiences 1 nanosecond of delay variation from day to day. These stability requirements drive the design of the RF downconverter and tracking loops of the GPS receivers.

To validate the GPS common-view error budget presented in Table 1 in a real-world application on continental baselines, Interstate has collected and analyzed data gathered over such a baseline. We combined data from a NIST GPS receiver situated at the Interstate Anaheim facility and the USNO GPS timing receiver in Washington, D.C. The data analysis took place at IEC, using the separation-of-variances technique and common-view data processing algorithms described in this paper. Fifty days of uninterrupted data concluding on MJD 47636 (20 April 1989) were examined to provide these results. The architecture of the NIST receiver is described in detail by Davis and others in Reference 3.

The GPS tracking schedule for this experiment exploited the repeating ground tracks of the Block I satellites. The new PRN 14 satellite was not used for the experiment due to control segment testing

during the data gathering interval. The schedule is given in Table 2. One notes the extremely low elevation of PRN 12 as seen at Interstate; its track time tends to fall during daytime here. The other tracks tend to occur at nighttime, reducing single-frequency ionosphere error. These times are shifted 4 minutes per solar day to follow the repeating ground track.

The NIST receiver at Interstate measured the phase of an HP 5061 cesium standard relative to GPS. The receiver at USNO provided the phase of UTC (USNO) relative to GPS; these data were downloaded from the USNO dial-up service. We examined the data for missing points. Any gaps were filled with linear interpolation of the local-SV and local-GPS measurements. Then the IEC-GPS and UTC-GPS measurements were differenced to produce six series of common-view GPS measurements of IEC-UTC (USNO) time differences. Each series consists of one time difference measurement per sidereal day from a given GPS satellite.

We analyzed the GPS common-view measurement tracks using the multicorner hat separation-of-variances software (described later in this paper) to produce estimates of the measurement noise found on each repeating measurement track. This makes the implicit assumption that all the variances are constant over the data interval. The noise introduced by each satellite path was estimated via a three-corner hat on the differences between IEC-UTC estimates on separate satellite paths. As the long-term GPS measurement noise has the characteristic of white phase modulation, we scale the Allan deviation by 86,160 seconds to obtain measurement noise filter values. The results are presented in Table 3. One quickly notes that PRN 12 measurements exhibited three times the noise seen on the other paths.

We next estimated the frequency stability of the IEC-UTC difference by applying the separation of variances to the local-GPS tracks. At an averaging time of one sidereal day, we observed stability of 1.03×10^{-13} . This value was used to adjust the common-view time transfer Kalman filter process noise matrix accordingly. We divide the Allan variance at one sidereal day by 86160 to produce the correct process noise matrix frequency noise parameter. Next, a two-state Kalman filter-smoother produced estimates of smoothed IEC-UTC phase and frequency offsets from each common-view track. We apply the smoother to each track individually. The effectiveness of the smoother can be seen by examining the smoothed residual root-mean-square values. The RMS of the difference between the raw common-view data and the smoothed estimates for all tracks is presented in table 4, along with the percentage of measurements accepted by the Kalman filter.

The final step in the time transfer consists of taking a weighted mean of the IEC-UTC phase estimates from the various GPS tracks. The weights are determined from the table 4 values to achieve optimal stability. Another weighted mean omitting PRN 12 was also taken due to the anomalous nature of the PRN 12 path. Figures 2 through 5 show each track's difference from the weighted mean in both cases. We clearly see the biasing of PRN 12 from the rest of the tracks. Its greater noise also compels the weighting algorithm to ignore that track when combining the satellite data. Therefore, comparison of the IEC-UTC (USNO) weighted averages between the two cases revealed differences of 1 nanosecond or less. As a measure of time transfer accuracy and consistency, the RMS of all tracks' differences from the weighted mean is computed by the weighting software. For the all-inclusive weighted mean, the RMS amounted to 13.02 nanoseconds. For the weighted mean omitting PRN 12, the RMS of the differences amounted to 5.6 nanoseconds. It is thus apparent that the results demonstrate the feasibility of 10-nanosecond time transfer using GPS over continental baselines. However, even more room for improvement exists. Improvements in surveying, ionospheric models, and antenna multipath resistance could lead to consistent nanosecond-level performances.

The stability of the IEC-UTC (USNO) difference as estimated by the GPS common-view process is presented in Figure 6. The differences were first fit to a quadratic to remove deterministic frequency bias and drift. The mean clock bias removed was -18069.99 ns. The mean frequency removed was -279.46 ns per sidereal day. The mean frequency drift was 0.0931 ns per sidereal day squared.

ZERO BASELINE TESTS MEASURE RECEIVER STABILITY

We can compute the long-term stability of collocated receivers by driving them off the same local frequency standard, comparing the time offset measurements from the two receivers, and computing the Allan two-sample variance from the data stream. The negligible baseline provides for complete GPS navigation message error cancellation. The errors due to survey and atmospheric modeling cancel if common values are used in both receivers. The remaining difference between the two local-GPS measurements in common view consists of the relative delay between the two receivers plus random error. By applying the smoothing technique described in this paper, we can quantify the long-term receiver delay stability.

Interstate has performed common-view time synchronization tests in the Anaheim laboratory that demonstrate this concept. The test compared the NIST receiver at IEC with a similar time transfer receiver, the Allen Osborne Associates TTR-6 model GPS receiver. We observed a 3.6 nanosecond standard deviation in unsmoothed GPS time differences. We also observed GPS receiver stability to 2 nanoseconds per day. Figure 7 presents the smoothed time differences taken over 40 days. Each point on the plot indicates the difference between the NIST receiver's estimate of local-GPS time bias and that from the Allen Osborne receiver. The mean value of these differences measures the uncompensated cable delays and receiver signal delays. The GPS common-view measurements represented in figures 8 and 9 are a composite of measurements from GPS satellite (PRN) numbers 3, 6, 9, 11, 12, and 13. The smoothed receiver delay comparisons reveal that the NIST and Osborne receivers both have long-term stability of less than one part in 10^{-14} for averaging times of one to eight days. Figure 10 indicates the long-term stability values.

MULTICORNER HAT ALGORITHMS CHARACTERIZE GPS NOISE

The multicorner hat concept overcomes a fundamental limitation of time and frequency measurements by introducing a third oscillator into the measurements to provide observability of each clock's Allan variance. Because oscillator phase measurements can be made only with respect to another clock, either clock could potentially cause the noise quantified by the Allan variances. To resolve which clock is "at fault," we introduce a third clock, then find Allan variances of all three possible differences. If the three clocks are independent, we may assume that the variance of the differences is the sum of the individual clock Allan variances. Three Allan variances of difference data permit us to solve for each clock's Allan variance, removing the effects of the other two clocks. By extending the three-corner hat concept to systems with multiple timing error sources, we can compute the stability of individual clocks within the GPS system. This concept, pioneered by Allan and Weiss in Reference 4, permits us to validate the stability of GPS time synchronization without having to develop and to implement elaborate system error models laden with free parameters. Figure 11 shows the steps performed in the multicorner hat separation of variances. We sort the GPS time difference data into measurements taken each sidereal day. The repeating GPS ground track permits us to eliminate systematic error creeping into the results by enforcing the same geometry on each common-view measurement. We then remove deterministic phase, frequency and frequency drift coefficients through a quadratic fit to the sidereal-day track data. Householder transformations used for the fit ensure numerical accuracy, as described by Bierman in reference 5. The residuals from this quadratic fit contain the random errors, which we can characterize through use of the multicorner hat concept.

We can take three types of time difference measurements with a GPS receiver: local-GPS, local-satellite, and GPS-satellite. Each satellite provides these measurements from each tracking interval.

We can decompose the errors in those measurements into their constituent parts:

- Local frequency standard instability,
- GPS ephemeris and atmospheric errors,
- GPS uploaded satellite clock correction errors,
- GPS master system time instability and
- Satellite oscillator instability.

We difference the local-GPS offset measurements from three satellites to isolate the combined noise due to ephemeris and clock correction error, then apply the three-corner hat to obtain the sum of the Allan variances due to those two error sources for each of the three satellites. The same technique applied to the local-satellite clock offset data produces the sum of the Allan variances of ephemeris and satellite hardware clock noises. We combine these preliminary three-corner hat results from a given satellite with the Allan variances of the original three measurement streams from that satellite to obtain the final separation of variances. We can express the Allan variances of the difference data in terms of their constituent parts, analogous to the three-corner hat. We then invert this expression to solve for the individual error source Allan variances, performing a five-corner hat for each of the three satellites used in the preliminary variance separations. This provides three estimates of local clock stability and GPS time stability that can be averaged to obtain the final stability estimates.

The multicorner hat procedure suffers from the possibility of computing negative variances for some of the stability estimates. Three potential causes of such results are (1) insufficient data to separate all variances; (2) unmodeled correlations between measurements; and (3) one of the clocks in the multicorner hat is much more stable than the others and is thus obscured by noise. We remedy the first problem by gathering more time difference data. The second problem can be solved by modeling correlation terms in the multicorner hat. The occurrence of the third problem indicates that clocks with greater stability are needed. In any case, the nonnegative variances can be accepted as good estimates of stability.

We can see the multicorner hat's applicability to general performance validation problems from the preceding discussions, particularly in navigation applications. Given three independent navigation systems we can compute the accuracy of each system by taking the sample variance of the mutual difference data, then applying the three-corner hat to the resulting values. This provides a prior-free system validation methodology. Extensions of the multicorner hat to include cross-correlation terms between navigation systems can estimate the effects of common system components. For example, if two aided inertial navigators share a common inertial unit but use different range aiding systems, then a correlation term can be added to the multi-corner hat. Extra differences are then required to separate all the variances.

Interstate applied the separation-of-variances technique described above to time difference data gathered in November 1988. Figures 12 to 15 show the excellent time stability of the various clocks in the GPS, as validated by the multicorner hat algorithms. The HP 5061B cesium beam standard exhibited frequency stability 50 times better than specified by the manufacturer, as shown in figure 12. GPS time showed comparable stability to that of the HP cesium in the IEC laboratory, as exhibited in Figure 13. In the short term, however, the HP outperformed the GPS in time stability. From this we can see that GPS time reaches a flicker noise frequency modulation floor of approximately 6×10^{-14} at an averaging time of 3 days.

Our multicorner hat approach allows us to show that in the GPS space segment, proper isolation of rubidium oscillators can provide an environment in which cesium-level performance results. Figure

14 indicates the excellent long-term stability of the cesium beam standard aboard the GPS PRN 3 satellite. A flicker floor of less than 3×10^{-14} occurred between averaging times of 4 and 8 days. In contrast, figure 15 shows that the performance of the GPS PRN 9 rubidium standard actually surpassed that of the spaceborne cesium at averaging times of 1 and 2 days. This short-term superiority is expected in rubidium standards and is further enhanced by the relatively benign environment of the GPS satellite. No apparent force acts on the satellite nor are there extreme temperature fluctuations, thus the usual causes of poor rubidium performance do not pervade the satellite environment. In addition, the PRN 9 rubidium has special heat-dissipation hardware that enhances its performance.

The GPS control segment can benefit from this research by using the multicorner hat approach as an independent performance monitor on the new Block II satellites. In addition, the concepts behind the multicorner hat have application in any performance validation problem where the accuracy of the references is of interest.

ACKNOWLEDGMENTS

The author would like to thank the following persons: Len Jacobson, Dr. Ken Brunn, and Gerry Grayson of Interstate for managerial support of this project; Tony Kurlovich of Interstate for RF receiver stability analysis; Randy Hom, Robert Crane, and Manny Beckers of Interstate for technical support; and David Allan, Marc Weiss, and Dick Davis of NIST for their interest and consulting services throughout the project.

REFERENCES

1. Allan, D. W., "National and International Time and Frequency Comparisons," Time and Frequency Division, National Institute of Standards and Technology, Boulder, CO.
2. Phase 1 Navstar/GPS Major Field Test Objective Report, Tropospheric Correction, Navstar/GPS Joint Program Office, Space and Missile Systems Organization, Los Angeles Air Force Station, Los Angeles, CA., 4 May 1979.
3. Davis, Dick D.; Weiss, Marc A.; Clements, Alvin C.; and Allan, David W., "Remote Synchronization Within a Few Nanoseconds by Simultaneous Viewing of the 1.575 GHz GPS Satellite Signals", Time and Frequency Division, National Institute of Standards and Technology, Boulder, CO.
4. Allan, D. W., and Weiss, M., "Separating the Variances of Noise Components in the Global Positioning System," Proceedings of the Fifteenth Annual Precise Time and Time Interval Applications and Planning Meeting, December 1983.
5. Bierman, G. J., "Factorization Methods for Discrete Sequential Estimation," Academic Press, New York, 1977.

NOTE: References 1, 3, and 4 are also available in documentation supplied as part of the NIST Time Dissemination Service.

Table 1. The GPS common-view error budget for continental distances shows the domination of satellite ephemeris error. For shorter baselines the orbital error contribution decreases significantly, increasing the potential accuracy.

Error Source	Contribution (ns)
Ephemeris	8.5
GPS receivers	4.9
Ionosphere	1.4
Troposphere	1.4
Relative Survey	<u>1.4</u>
Root-Sum-Square Total	10.1 ns

Table 2. GPS tracking schedule 20 April 1989 shows geometry of common-view measurements.

PRN No.	Time of Track (Zulu)	IEC		USNO	
		Elevation (deg)	Azimuth (deg)	Elevation (deg)	Azimuth (deg)
3	7:18	50	40	61	340
6	2:22	60	124	62	242
9	3:12	88	273	47	288
11	3:56	38	31	58	351
12	13:18	21	61	60	90
13	5:28	44	30	56	342

Table 3. Common-view measurement noise estimates from multicorner hat show poor PRN 12 performance.

PRN No.	One-Day Allan Variance	Equivalent Measurement Variance (ns ²)	Noise Sigma (ns)
3	1.14×10^{-26}	84.63	9.20
6	6.33×10^{-27}	46.99	6.85
9	8.40×10^{-27}	62.36	7.90
11	8.17×10^{-27}	60.65	7.78
12	8.16×10^{-26}	605.76	24.61
13	8.70×10^{-27}	64.58	8.04

Table 4. Common-view smoothed residual RMS values indicate higher noise on PRN 12 path.

PRN No.	Smoothed RMS Variance	Percentage Accepted
3	5.31	100
6	4.73	100
9	5.43	100
11	5.37	100
12	11.30	100
13	4.45	100

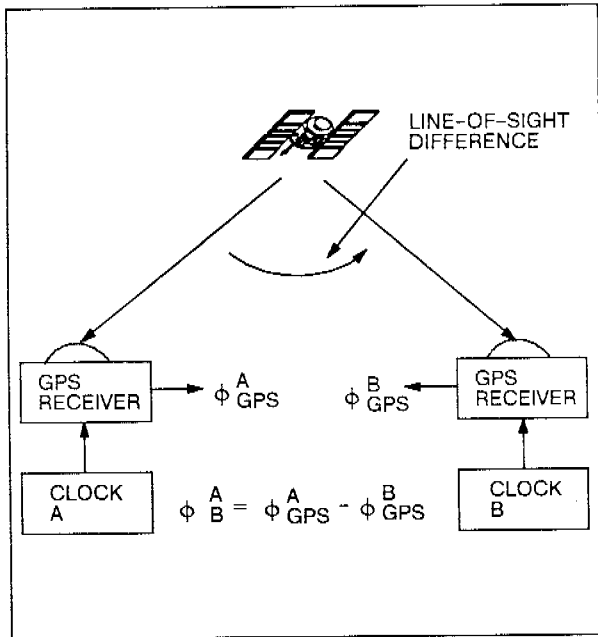


Figure 1. Common-view GPS provides high ephemeris error cancellation, permitting time transfer to nanoseconds of error.

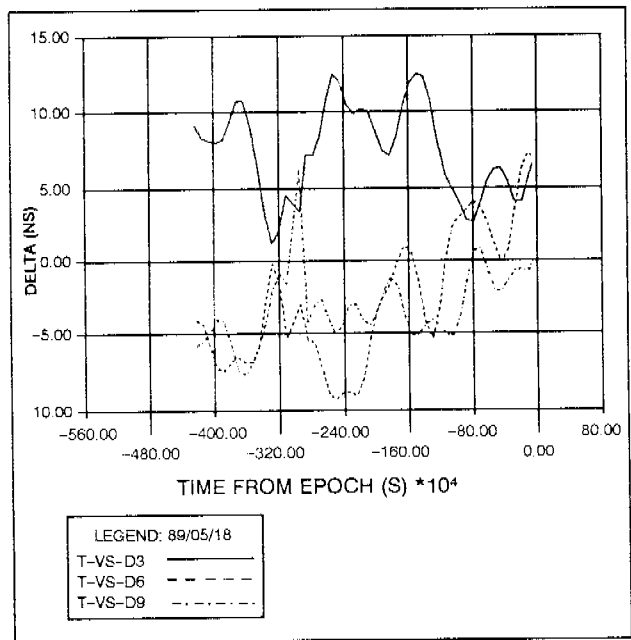


Figure 2. Differences from weighted mean for PRNs 3, 6, and 9 show agreement to 5 nanoseconds RMS.

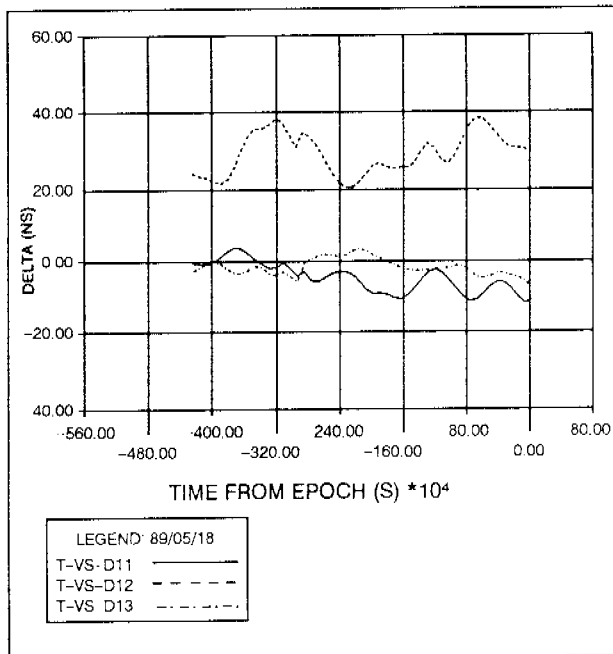


Figure 3. Weighted mean differences clearly indicate biaslike error in PRN 12 track. Extra noise is also evident.

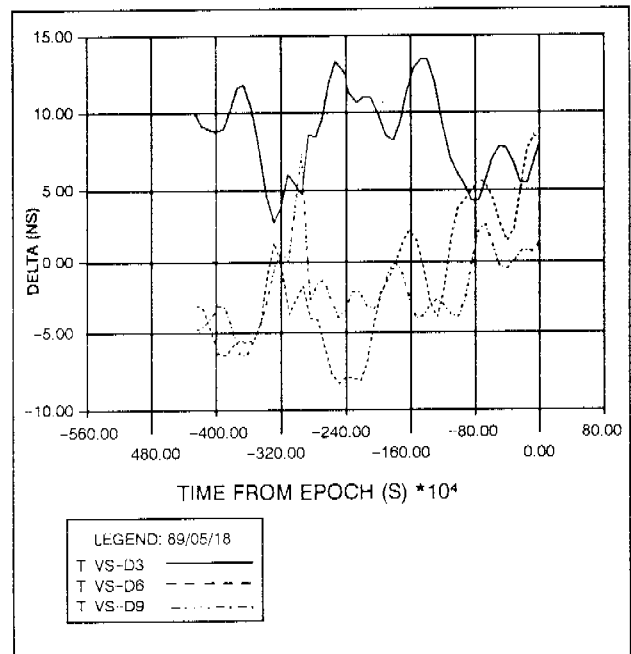


Figure 4. Excluding PRN 12 produced only 1-nanosecond change in weighted mean differences.

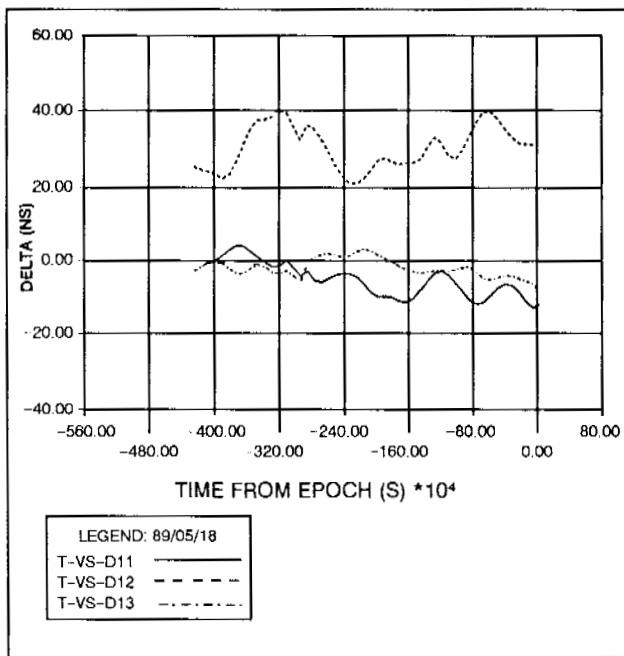


Figure 5. All-inclusive weighted mean ignores PRN 12, as shown by little change in differences when PRN 12 is excluded.

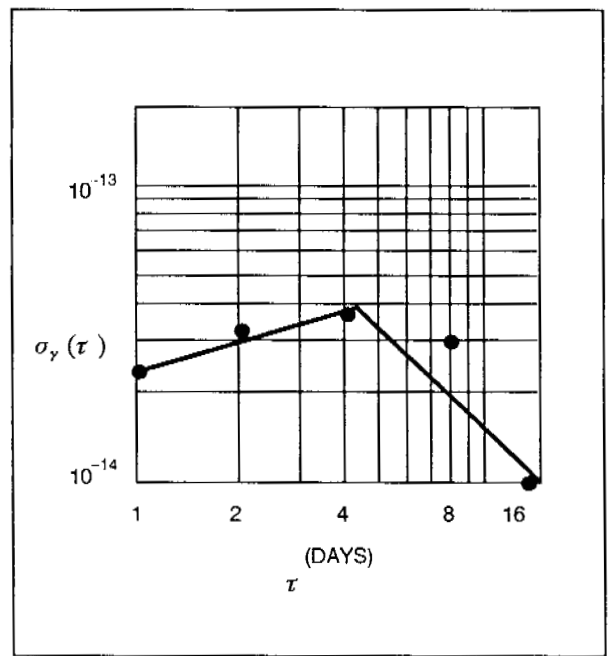


Figure 6. An HP 5061B cesium at Interstate exhibits excellent smoothed frequency stability versus UTC (USNO).

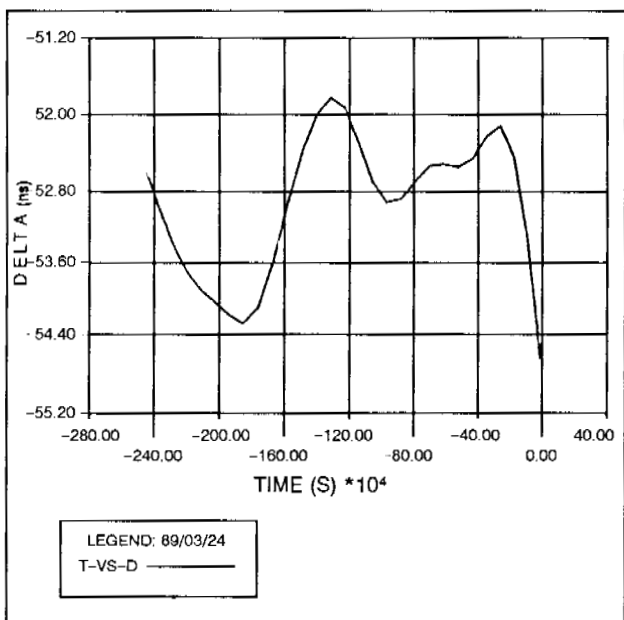


Figure 7. Common-view weighted mean error shows 0.7-nsec deviation.

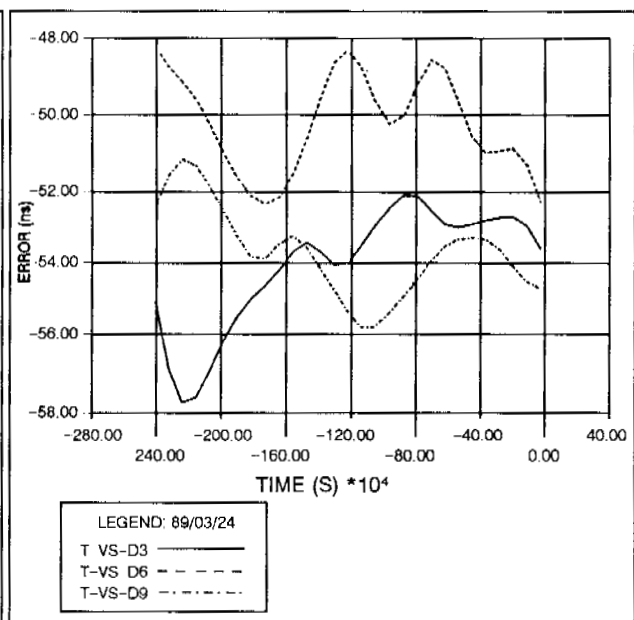


Figure 8. Common-view smoothed tracks show satellite-by-satellite deviations for PRNs 3, 6 and 9.

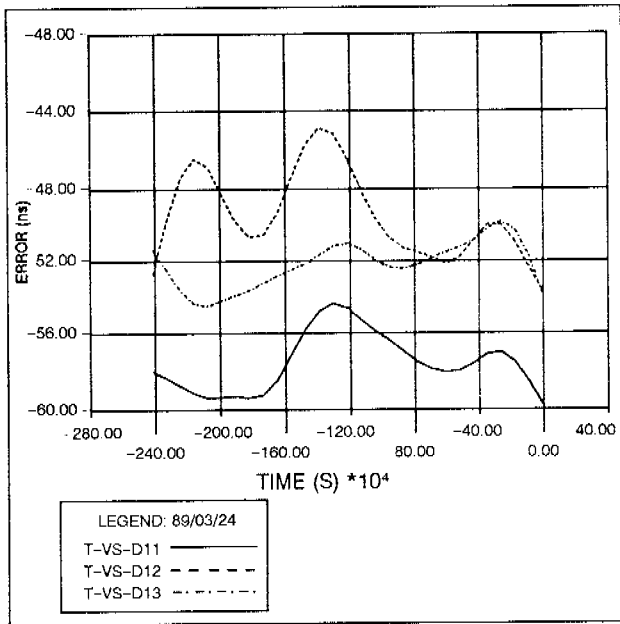


Figure 9. Common-view smoothed tracks show satellite-by-satellite deviations for PRNs 11, 12, and 13.

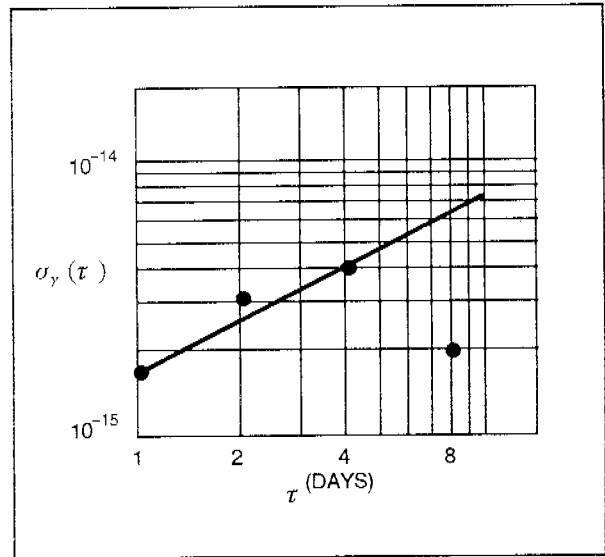


Figure 10. Smoothed receiver time stability is less than one part in 10^{14} .

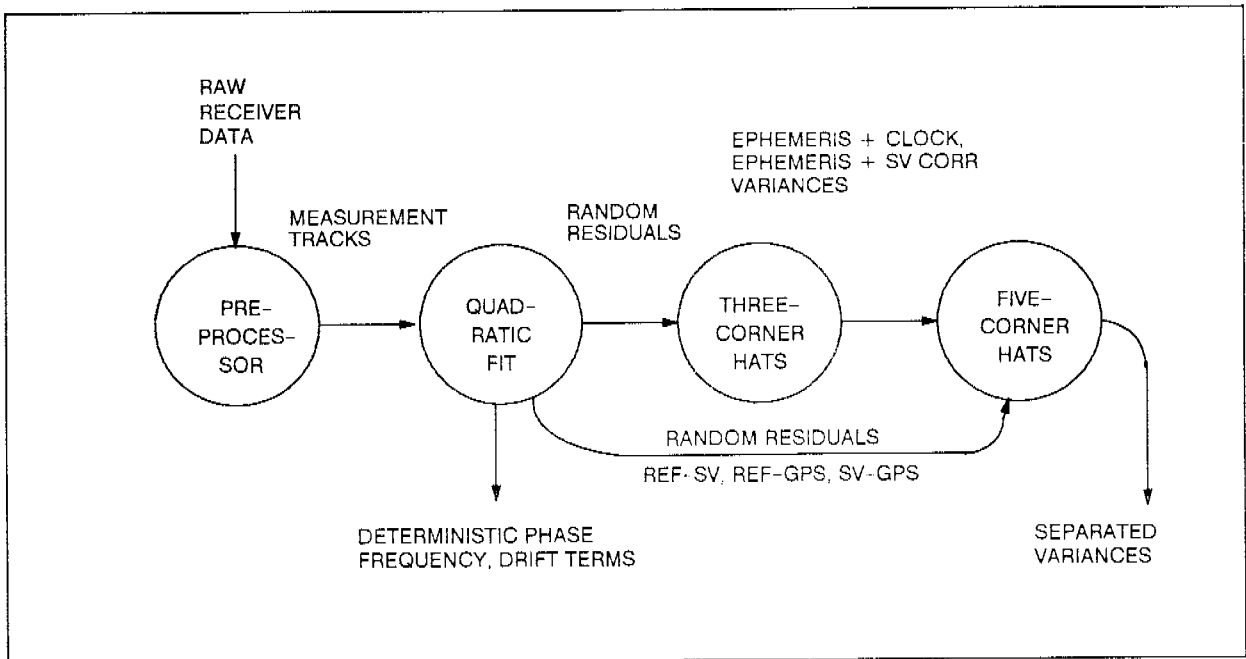


Figure 11. Data flow shows procedure for multicorner hat.

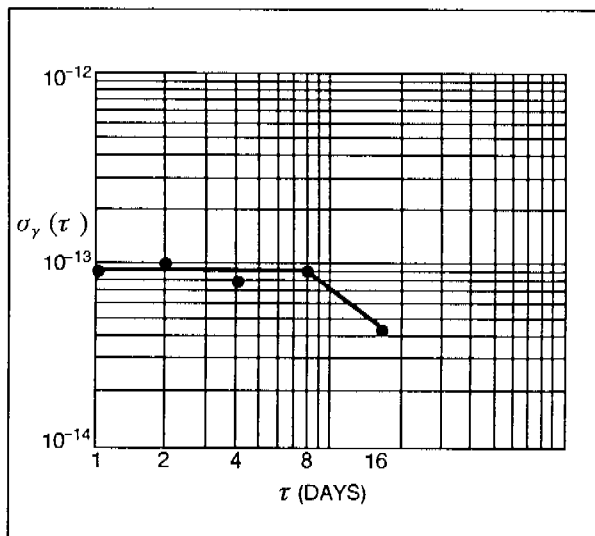


Figure 12. Standard HP 5061B cesium shows performance fifty times better than specification.

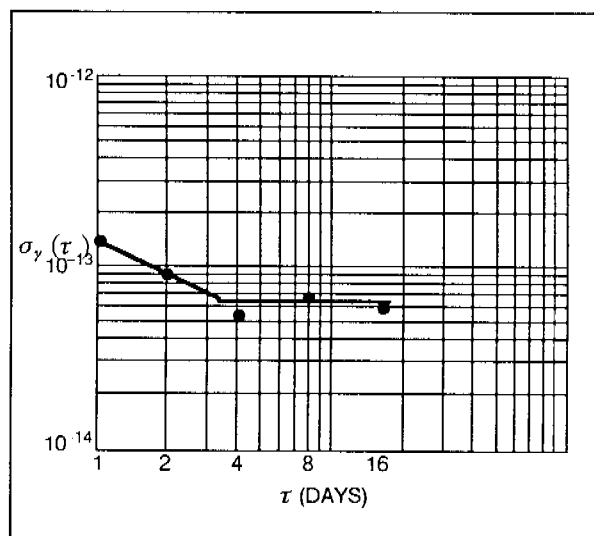


Figure 13. GPS master control segment clock reaches flicker floor at 4 days.

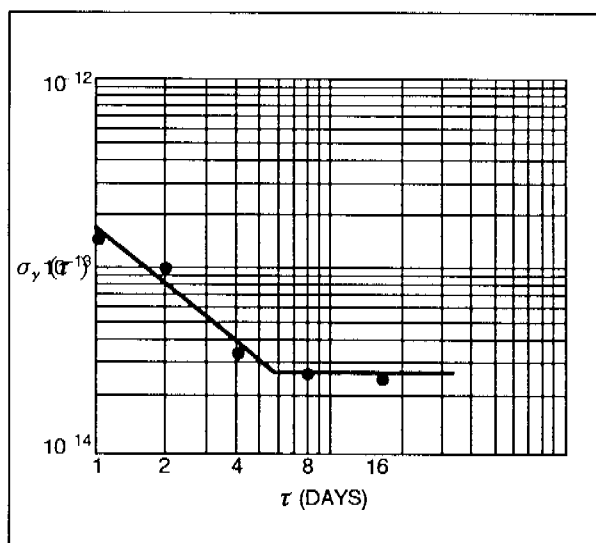


Figure 14. SV 3 cesium shows excellent long-term stability.

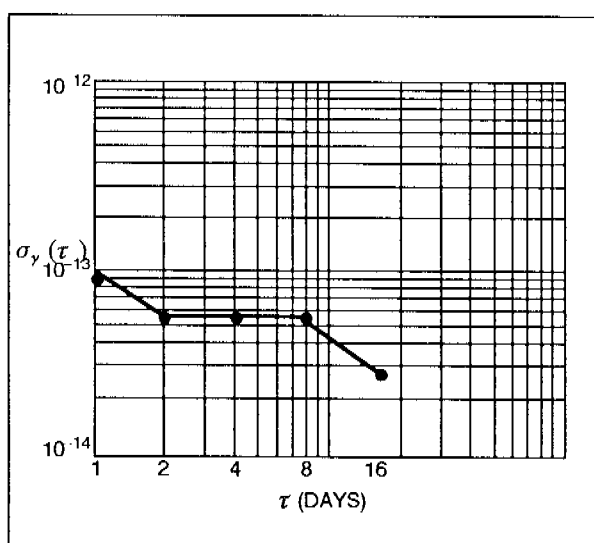


Figure 15. SV 9 rubidium performs better than cesium in short term.